Temperature dependence of the kinetic energy in condensed argon

M. A. Fradkin* and S.-X. Zeng
Physics Department and Frederick Seitz Materials Research Laboratory, University of Illinois at Urbana-Champaign, Urbana, Illinois 61801-3080

R. O. Simmons†
Sektion Physik, Ludwig-Maximilians-Universität München, D-80539 München, Germany
(Received 8 July 1993; revised manuscript received 18 October 1993)

Using eV neutron scattering, direct measurements have been made of the average single-particle kinetic energies, $\langle E_k \rangle$, for a series of condensed Ar samples over the range 18–85 K. These temperature-dependent measurements are on a system with $A > 22$ amu in the regime below equipartition. The scattering from liquid-Ar samples, for which it is assumed that $\langle E_k \rangle$ can be determined with sufficient accuracy from a quantum expansion, has been used to provide information about the total corrections to be made to account for neutron time-of-flight spectrometer resolution and multiple scattering. Data were obtained for wave-vector transfers in the range 192–254 nm^{-1}, to check for possible systematic contributions to experimental uncertainty. The directly measured $\langle E_k(T) \rangle$ is compared to expectations from thermodynamic experiments, from previous neutron-scattering measurements of collective vibrational modes of the solid, and from various theoretical models. The directly measured temperature dependence provides evidence for use in the interpretation of other experiments which use Ar as an "inert" host.

I. INTRODUCTION

Pulsed neutron sources, with appreciable epithermal fluxes, and associated neutron spectrometers invite the exploration of neutron scattering as a probe of single-particle excitations in condensed matter. The single-particle kinetic energy, $\langle E_k \rangle$, has previously been inaccessible to direct measurement (indirect inferences have been available from phonon spectra and Debye-Waller factors). The majority of experimental work on condensed noble gases has been focused on ^{4}He phases due to their rich behavior. There has been little research on single-particle excitations in the heavier noble gas solids Ar, Kr, and Xe other than near their respective triple points.[1,2] In some sense this is surprising since Ar in particular has long been a fertile testing ground for theoretical models due to the supposed simplicity of its interatomic interactions.[3]

The present work explores the possibility of quantitative measurement of the temperature dependence of $\langle E_k \rangle$ in condensed Ar.[4] Ar is an ideal substance for such a test because excellent thermodynamic data plus partial neutron-scattering information (for small wave-vector transfers $\mathbf{Q}$) already exist. The thermodynamic data include measurements of the macroscopic specific heat, thermal expansion, bulk modulus, and pressure versus volume, plus information about the elastic constants at extremely high temperatures.[3] Various coherent inelastic-neutron-scattering studies of solid Ar have been published.[5–7] We compare our results for $\langle E_k(T) \rangle$ to predictions of quasiharmonic Born–von Kármán fits to measured phonon dispersion in Ar and to various theories. Finally, in the Appendix we point out the difference between $\langle E_k(T) \rangle$ and the mean-squared displacement, $\langle u^2(T) \rangle$, which appears in the Debye-Waller factor.

II. EXPERIMENTAL METHOD

A. Neutron scattering at large Q

For a system of N identical target atoms the inelastic double differential cross section for the scattering of neutrons can be written as[8]

$$\frac{d^2\sigma}{d\Omega d\omega} = Nb^2 \left[\frac{k_f}{k_i} \right] S(\mathbf{Q},\omega) , \tag{1}$$

where b is the scattering length, k_f and k_i are the magnitudes of the final and initial neutron wave vectors, respectively, $\mathbf{Q}$ is the wave-vector transfer defined by $\mathbf{Q}=\mathbf{k}_i-\mathbf{k}_f$, and $E=\hbar\omega$ is the energy transferred to the target particle by the neutron during the scattering process. $S(\mathbf{Q},\omega)$, the dynamic structure factor, has the general form

$$S(\mathbf{Q},\omega) = \frac{1}{2\pi} \int_{-\infty}^{+\infty} F(\mathbf{Q},t) \exp(-i\omega t) dt , \tag{2}$$

with

$$F(\mathbf{Q},t) = \frac{1}{N} \sum_{ij} \langle \exp[-i\mathbf{Q}\cdot\mathbf{R}_i(0)] \exp[i\mathbf{Q}\cdot\mathbf{R}_j(t)] \rangle , \tag{3}$$

where $\mathbf{R}_i$ is the atomic position operator of the ith atom in the Heisenberg picture, and $\langle \cdots \rangle$ indicates a thermal average. In the limit of large wave-vector transfer $\mathbf{Q}$, incident neutrons scatter from individual nuclei indepen-

dently and therefore respond only to the atomic single-particle momentum distribution, $n(\mathbf{p})$. In this limit, known as the impulse approximation (IA), the dynamic structure factor assumes the simple form

$$S_{\mathrm{IA}}(\mathbf{Q},\omega)=\int_{-\infty}^{+\infty} n(\mathbf{p})\delta\left[\omega-\omega_R-\frac{\mathbf{Q}\cdot\mathbf{p}}{M}\right]d^3p \ , \quad (4)$$

where the $n(\mathbf{p})$ satisfies the normalization condition

$$\int_{-\infty}^{+\infty} n(\mathbf{p})d^3p=1 \ , \quad (5)$$

and the average recoil energy transferred to a target particle by an incident neutron is

$$\hbar\omega_R=\frac{\hbar^2Q^2}{2M} \ , \quad (6)$$

where M is the mass of the scatterer. The argument of the δ function expresses conservation of energy and momentum for the scattering process. Once $n(\mathbf{p})$ is known from measurement of the $S(\mathbf{Q},\omega)$, the single-particle kinetic energy, $\langle E_k\rangle$, can be determined by integration over all atomic momenta weighted by the momentum distribution

$$\langle E_k\rangle=\int_{-\infty}^{+\infty} n(\mathbf{p})\frac{p^2}{2M}d^3p \ . \quad (7)$$

For an isotropic Gaussian momentum distribution

$$n(p)\propto\exp\left[\frac{-p^2}{2\sigma_p^2}\right] \ , \quad (8)$$

$S_{\mathrm{IA}}(Q,\omega)$ is also Gaussian in form with its center located at the recoil frequency,

$$S_{\mathrm{IA}}(Q,\omega)\propto\exp\left[\frac{-M^2(\omega-\omega_R)^2}{2Q^2\sigma_p^2}\right] \ , \quad (9)$$

and $\langle E_k\rangle$ is given by

$$\langle E_k\rangle=\frac{3\sigma_p^2}{2M} \ . \quad (10)$$

It has become standard in deep-inelastic-neutron scattering to present the data in terms of the longitudinal momentum distribution function $J(y)$ rather than $S(Q,\omega)$. The relationship between the two quantities for an isotropic system, such as a liquid, gas, or polycrystalline specimen, is

$$J(y)=\frac{Q}{M}S(Q,\omega) \ , \quad (11)$$

with the scaling variable y defined as

$$y=\frac{M}{\hbar Q}(\omega-\omega_R) \ . \quad (12)$$

In the IA, $J(y)$ is Gaussian if the momentum distribution is Gaussian. The single scaling variable y expresses the fact that at large Q, where Eq. (4) is valid, the scattering function is characterized by its width alone, and that width is determined only by $\langle E_k\rangle$ and Q. For a system composed of several types of nuclei scattering independently, the observed response in the IA is the sum of individual responses.

The regime of applicability of the IA is a matter of some debate. Various theoretical approaches have been developed to account for deviations from the IA, known as a final-state effects, in deep-inelastic scattering data.[8,9] In Sears' treatment,[8] deviations from IA behavior are expressed in an asymptotic expansion of symmetric and antisymmetric terms

$$J_o(y)=J_{\mathrm{IA}}(y)-A_3\left[\frac{d^3J_{\mathrm{IA}}(y)}{dy^3}\right]+A_4\left[\frac{d^4J_{\mathrm{IA}}(y)}{dy^4}\right]-\cdots \ , \quad (13)$$

where $J_o(y)$ is the observed $J(y)$ (neglecting the effects of instrument resolution) and $J_{\mathrm{IA}}(y)$ is $J(y)$ in the IA. In this expansion the coefficients are Q dependent. In particular, the coefficient of the first antisymmetric term A_3 and the coefficient of the first symmetric term A_4 in the expansion are

$$A_3=\frac{M\langle\nabla^2V\rangle}{36\hbar^2Q} \quad \text{and} \quad A_4=\frac{M^2\langle\mathbf{F}^2\rangle}{72\hbar^4Q^2} \ , \quad (14)$$

where V is the interatomic pair potential and $\langle\mathbf{F}^2\rangle$ is the mean-squared force on the target atom arising from its interaction with neighboring particles.

Our assumption that $n(p)$ has a Gaussian form is supported by the result that for harmonic systems, systems for which the central limit theorem is valid, and for classical systems with velocity independent interatomic forces, $n(p)$ is Gaussian.[10] At higher temperatures, quantum effects are small and solid Ar is expected to display essentially classical behavior. At low temperatures non-Gaussian contributions to $n(p)$ are expected to be negligible; Hartree calculations of the ground-state wave function in solid Ar yield, for a spherically symmetric wave function, a Gaussian.[11]

B. Spectrometer

Our measurements used the LRMECS spectrometer at Argonne National Laboratory's Intense Pulsed Neutron Source (IPNS). At IPNS neutrons were produced through spallation by bombarding an enriched uranium target with 30-Hz pulses of 500-MeV protons. Initial energy selection was carried out by a Fermi chopper phased to the proton pulses. The incident neutron energy was determined by time-of-flight with two low-efficiency BF_3 monitors, one located 46 cm upstream of the sample chamber the other located 325 cm downstream of the sample chamber. Neutrons scattered by the sample were detected by ^{3}He detectors located approximately 2.5 m from the sample position over an angular range of 72–117 degrees. The final neutron energy was determined via time-of-flight. For data analysis purposes the detectors were group in four banks having mean scattering angles of 112.6°, 101.2°, 88.8°, and 77.4°. At the nominal incident neutron energy used in our measurements, 500 meV, these banks correspond to average

wave-vector transfers of 254, 236, 215, and 192 nm^{-1}, respectively. Problems arose with several detectors in the 88.8° bank during several of the runs, hence for the three lower-temperature samples the 88.8° bank was excluded from the analysis.

C. Measurement conditions

The samples were prepared *in situ* with a clean gas-handling system by condensing research grade natural Ar (stated purity 99.999%), obtained from the Linde Division of Union Carbide. The relative natural abundances and neutron-scattering properties of the stable isotopes of Ar are shown in Table I. While ^{36}Ar constitutes only a small fraction of natural Ar, due to its large neutron-scattering cross section, approximately 38% of the scattering from natural Ar is due to ^{36}Ar.

The sample cell consisted of four vertical tubes constructed of 6061-T6 aluminum, 1.9 cm in outer diameter with a nominal wall thickness of 0.03 cm. Each tube exposed 10.2 cm to the incident beam. Cell temperatures were maintained by a Displex closed-cycle refrigeration system. For the three colder samples the temperature was measured with two Lake Shore Si diode thermometers, located at the top and the bottom of the sample cell. A Pt resistance thermometer was used for the three higher-temperature samples. Data collection for each condensed specimen took approximately 30 h. An empty cell run of the same length was taken in order to perform the primary background subtraction. The specified sample temperatures are averages. The temperature difference across the rather large cell never exceeded 1.4 degrees.

Due to the ramified cell geometry we presume the solid specimens were polycrystalline, with a range of crystalline orientations, and therefore our results apply to an angular average over all crystal directions in the fcc lattice. Neutron-diffraction measurements of solid ^4He samples in aluminum cells of a similar size and type reveal polycrystalline specimens.[12] ^4He generally grows larger crystallites than do the heavy noble gases.[13]

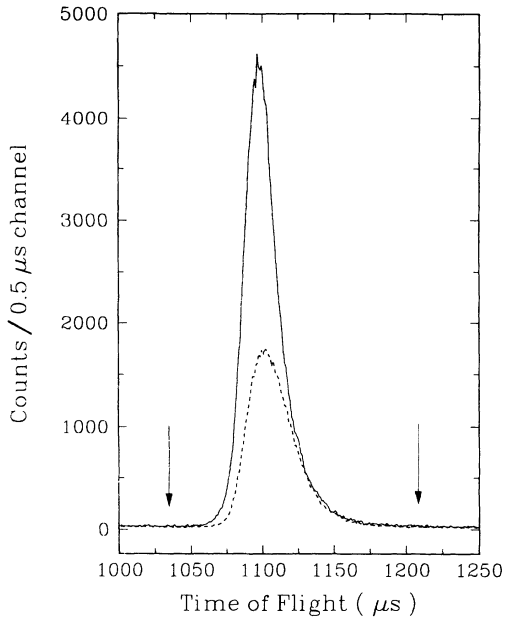

FIG. 1. Raw time-of-flight data for scattering into the 112.6° detector bank for liquid Ar at 110.6 K. The solid line is the signal due to the liquid Ar *and* the Al alloy sample cell. The dashed line is the signal from the empty cell, scaled using the data obtained from the upstream beam monitor. The difference between the two curves represents the response of the liquid Ar and any sample-dependent multiple scattering. This figure illustrates a difficulty to be overcome in these measurements: significant overlap of the Ar and cell scattering, because Ar and Al have somewhat similar masses. The arrows indicate the fit interval in time-of-flight and correspond to y values of ± 1000 nm^{-1}.

III. DATA ANALYSIS

Time-of-flight neutron data collected at the various detectors need to be corrected, in a primary manner, by subtraction of background measurements made with an empty cell (see Fig. 1). In addition to finite instrument resolution there are secondary backgrounds which need to be taken into account. These secondary backgrounds consist of multiple scattering including not only multiple scattering within the specimen itself but also such scattering in which one event occurs in the sample and another from some component of the spectrometer such as a vacuum hat, thermal radiation shield, etc. Because of the diversity of scattering agents, and the myriad of possible trajectories for multiply scattered neutrons, simulation of such scattering is nontrivial. Sophisticated computer simulations[12] are becoming available which allow the multiple-scattering backgrounds and instrument resolution to be calculated when the instrument and experimental geometry are well characterized. We developed an alternative precise method to account for secondary backgrounds and finite instrument resolution in our data.

TABLE I. Some properties of Ar isotopes. σ_s is the incoherent neutron-scattering cross section.

Isotope	Abundance (%)[a]	Mass[a]	σ_s [b]	Scattering intensity (%)
^{36}Ar	0.337	35.968 amu	77.9 barns	38.4
^{38}Ar	0.063	37.963	1.5	0.1
^{40}Ar	99.600	39.962	0.4	61.5

[a]Data taken from F. W. Walker, D. G. Miller, and F. Feiner, *Chart of the Nuclides,* 13th ed. (General Electric Company, San Jose, 1983).

[b]V. F. Sears, in *Methods of Experimental Physics,* edited by K. Sköld and D. L. Price (Academic, Orlando, 1986), Vol. 23A, p. 534.

This new method involves the use of a semiempirical fitting function, and works with less well-characterized situations.

This semiempirical method relies on quantitative comparison to results in the liquid state measured in identical geometry. For our reference Ar liquid, final-state effects are small and the single-particle kinetic energy can be determined by means of the Wigner expansion[14]

$$\langle E_k \rangle = \tfrac{3}{2} k_B T_{\text{eff}} , \tag{15}$$

where the effective temperature T_{eff} is related to the physical sample temperature T by

$$T_{\text{eff}} = T\left\{1+\left[\frac{1}{12}\right]\left[\frac{\theta}{T}\right]^2-\cdots\right\} . \tag{16}$$

with

$$\theta^2=\frac{\hbar^2\langle\nabla^2 V\rangle}{3Mk_B^2} . \tag{17}$$

In order to estimate the average value of the Laplacian of the interatomic potential that appears in Eq. (17) we used molecular-dynamics calculations of Verlet[15] for a Lennard-Jones fluid. These in conjunction with usual Lennard-Jones parameters[16] ($\varepsilon/k_B=119.8$ K, $\sigma=34.05$ nm) yield effective temperatures of 112.7 and 90.6 K for our 110.6- and 87.4-K liquid-Ar samples, respectively.

With the assumption of a Gaussian $n(p)$ and the $\langle E_k \rangle$ values of four liquid samples determined from Eqs. (15)–(17) we used the following prescription to generate fitting functions

$$J_o(y)=\int F(y-y')J_{\text{IA}}(y)dy' . \tag{18}$$

$J_o(y)$ is the measured liquid-Ar $J(y)$, $J_{\text{IA}}(y)$ is a Gaussian whose width is determined using Eqs. (15)–(17) and whose center is at $y=0$ nm^{-1}. The resulting fitting functions, $F(y-y')$, were essentially independent of the range of integration in Eq. (18) for choices from ± 750 to ± 1000 nm^{-1}, both well outside the range of detectable $J(y)$. The fitting function satisfies the normalization condition

$$\int F(y-y')dy'=1 . \tag{19}$$

The fitting functions are composed of three Gaussians whose widths, amplitudes, and center positions were varied to obtain the best fit with $J_o(y)$ when convoluted with $J_{\text{IA}}(y)$. Fitting functions composed of more than three Gaussians tended not to be smooth while those composed of fewer than three did not fit the data as well as three Gaussians. Because instrument resolution varies with scattering angle as do the secondary backgrounds, fitting functions were generated for each detector bank. The fitting functions thus determined account for finite instrument resolution and most of the sample-dependent multiple scattering for the *solid samples*, since the experimental circumstances of the solid samples were identical to those of the liquid samples in all respects save sample temperature and density.

As noted earlier most of the neutron scattering from a natural Ar sample is due to the isotopes ^{36}Ar and ^{40}Ar. In converting our raw time-of-flight data to $J(y)$ a cross-section weighted mass (38.42 amu) was used. Due to the large width of the observed liquid-scattering data, the longitudinal momentum distribution function for the liquid samples, used in the determination of the fitting functions, was treated as the response of a collection of identical scatterers having the cross-section weighted mass.

It is evident from Figs. 2 and 3 that our fitting functions are asymmetric. This is consistent with calculations, for a point scatterer, of pulsed-source neutron chopper spectrometer instrument resolution. Loong, Ikeda, and Carpenter[17] determined that the resolution functions characteristic of such instruments are asymmetric at all energies. Furthermore, the results of these calculations display a sharper falloff on the high-energy-transfer side, positive y, of the resolution function. This is similar to the behavior we observe in our semiempirical fitting functions at higher scattering angles and similar to the results of Monte Carlo simulations of chopper-spectrometer instrument resolution.[12] The fitting functions used in the analysis of the three higher-temperature samples differ somewhat for those applied to the three colder samples. This difference may arise due to differences in the cell orientation relative to the incident neutrons for the high- and low-temperature condensed samples.

Instrument resolution is the dominant component of our fitting functions due to the weak scattering nature of our sample and the physical characteristics of the spectrometer. The beam monitor data indicates the condensed specimens scattered approximately 4% of the incident neutrons. On LRMECS, the fitting function width is comparable to the width of our scattering data. This presents some difficulty in extracting $J(y)$, since the intrinsic line shape is significantly broadened and therefore rather good knowledge of instrument response is neces-

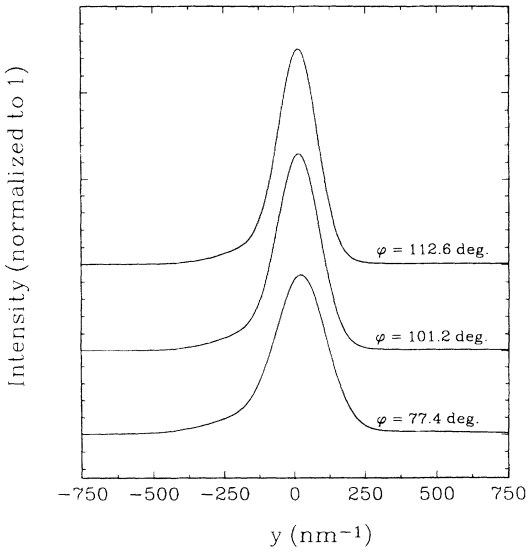

FIG. 2. Semiempirical fitting function derived from the 110.6-K liquid-Ar data for the 112.6°, 101.24°, and 77.4° detector banks with mean wave-vector transfers of 254, 236, and 192 nm^{-1}, respectively (see text Sec. III).

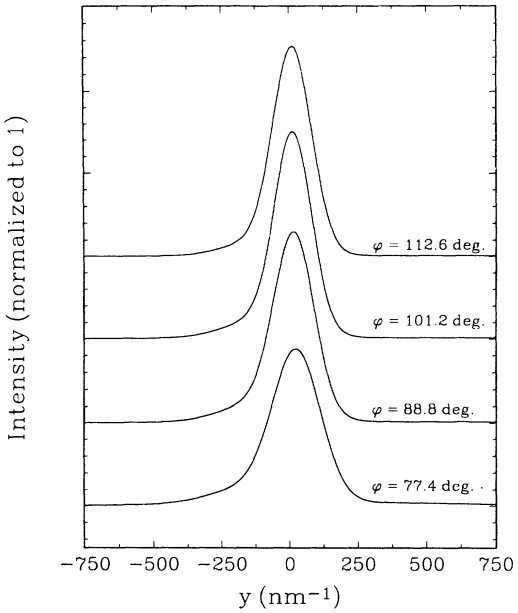

FIG. 3. Semiempirical fitting function derived from the 87.4-K liquid-Ar data for the 112.6°, 101.24°, 88.8°, and 77.4° detector banks with mean wave-vector transfers of 254, 236, 215, and 192 nm^{-1}, respectively (see text Sec. III).

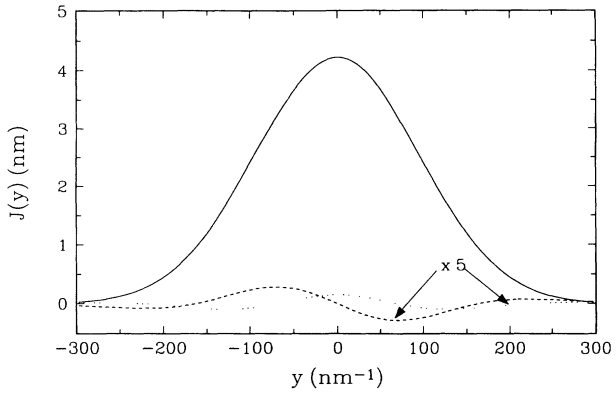

FIG. 4. Calculated $J(y)$ for liquid Ar at 110.6 K at a wave-vector transfer of 192 nm^{-1}. The dashed line represents the part of the response arising from the A_3 term in the Sears expansion, the dotted line represents the part due to the A_4 term [see Eqs. (13) and (14)]. The effect of instrument resolution has not been included. Note: The contributions due to the A_3 and A_4 terms have been *enlarged by a factor of 5* to aid their visibility.

sary to obtain accurate $\langle E_k \rangle$ values. We believe our semiempirical method, which is essentially based on a measurement of the instrument resolution function for the liquid samples plus the effects of sample-dependent multiple scattering, provides a sufficiently accurate description of instrument response.

One of the assumptions of our fitting function method is that final-state effects in the liquid samples are negligible. Justification for this is provided by the Sears expansion Eqs. (13), and (14), which is convergent for liquid Ar for our Q's. At our minimum Q, 192 nm^{-1}, we calculate, for the 110.6-K liquid-Ar sample, the absolute value of the first antisymmetric term at its maximum to be approximately 1.8% of $J_{IA}(y)$ at that value of y. At $y=0$ nm^{-1}, the first symmetric term is only 0.7% of $J_{IA}(y)$. Corrections of this size leave the width, and hence $\langle E_k \rangle$, essentially unchanged from that of $J_{IA}(y)$. This can be seen in Fig. 4, in which we have plotted three curves; (i) $J_{IA}(y)$, a Gaussian function with a width corresponding to an *effective* temperature of 112.7 K, (ii) the first antisymmetric term in the Sears expansion, and (iii) the first symmetric term in the Sears expansion. It should be noted that in Fig. 4 both these terms have been *enlarged by a factor of 5* to aid visibility. Due to the small size of these terms the expected measured $J(y)$, consisting primarily of $J_{IA}(y)$ and these correction terms, would not be visibly different from $J_{IA}(y)$ shown in Fig. 4. For the lower-temperature reference liquid sample (87.4 K) for the minimum Q of 192 nm^{-1}, the absolute value of the first antisymmetric term is 2.9% of $J_{IA}(y)$ at that value of y, while the first symmetric term is 1% of $J_{IA}(y)$ at $y=0$ nm^{-1}. We have also neglected the contribution of final-state effects in the scattering from this sample.

In order to determine the momentum distributions of the condensed specimens the fitting functions were convoluted with a model $J(y), J_m(y)$, which was varied to obtain the best fit to the measured $J(y)$,

$$J_o(y)=\int_{y_{\min}}^{y_{\max}} F(y-y')J_m(y')dy' \ . \tag{20}$$

Here $J_o(y)$ is the measured Ar $J(y)$, $y_{\min}=-750$ nm^{-1}, and $y_{\max}=+750$ nm^{-1}. Fitting over a larger y range ($-1000-+1000$ nm^{-1}) did not affect the results for $\langle E_k \rangle$. In our analysis of all condensed Ar samples we used a $J_{IA}(y)$ composed of two Gaussians in order to represent the individual scattering response of ^{36}Ar and ^{40}Ar. Fits to the 101.2° data are shown in Figs. 5–10. The mean wave-vector transfer at 101.2° is 236 nm^{-1}, however it should be noted that the wave-vector transfer changes by approximately ±10% across the peak. The fit residuals displayed in Figs. 5–10 are the difference between the data points and the fit, divided by the uncertainty associated with data points. As can be seen the fits are very good. Additional fits including an antisymmetric term having the same form as the first term in the Sears expansion did not unambiguously indicate the presence of final-state effects, which is consistent with our expectations from Fig. 4.

Additional justification for assuming final-state effects are negligible in the solid phase is that a multiphonon expansion of the scattering from a harmonic crystal indicates the scattering approaches the IA when the Debye-Waller factor is much less than one[18]

$$\exp\left[\frac{-Q^2\langle u^2\rangle}{3}\right] \ll 1 \ . \tag{21}$$

In the IA the target atoms scatter independently of one another, hence the Debye-Waller factor must be very small so there is no coherent scattering. Since Q is a measured quantity in our scattering experiment, knowledge of the atomic mean-squared displacement,

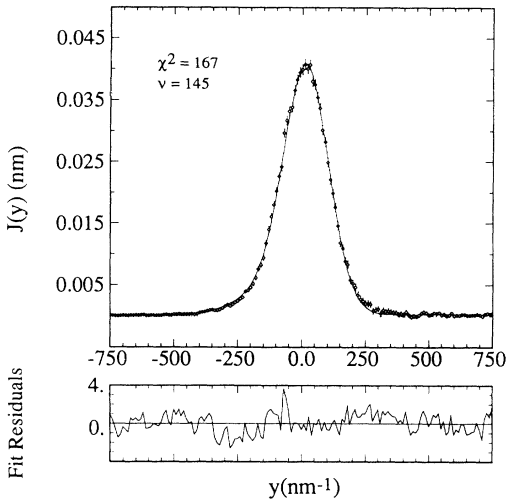

FIG. 5. Data from one detector bank (101.2°) for the momentum distribution of solid Ar at 18.3 K. The fitting procedure is described in Sec. III. ν is the number of degrees of freedom of a nonlinear least-squares fit. Note that the differences between data and fit are distributed uniformly throughout the range of y. For each sample temperature, data from three other detector banks were fitted similarly.

$\langle u^2 \rangle$, is needed to evaluate Eq. (21) and determine whether the wave-vector transfers reached in our experiments satisfy this inequality.

Because there are no measured mean-squared displacements for solid Ar, one must turn to theoretical calculations of this quantity.[19] Several methods have been employed to compute $\langle u^2 \rangle$ in solid Ar as a function of temperature. These include quasiharmonic calculations in which the second-order force constants are dependent upon strains and volume changes,[20] self-consistent phonon calculations (SCP),[21] and classical Monte Carlo and molecular-dynamics calculations.[22] Only the SCP calculations, however, yield reasonable values of $\langle u^2 \rangle$ for

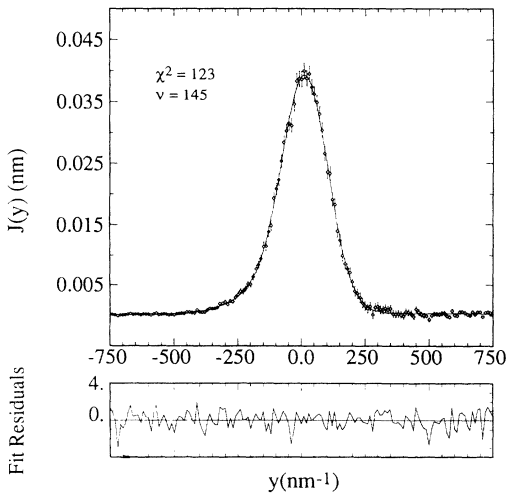

FIG. 6. 101.2° data and fit for solid Ar at 28.2 K. Again, note that no systematic deviations between data and fit are visible throughout the fitting range.

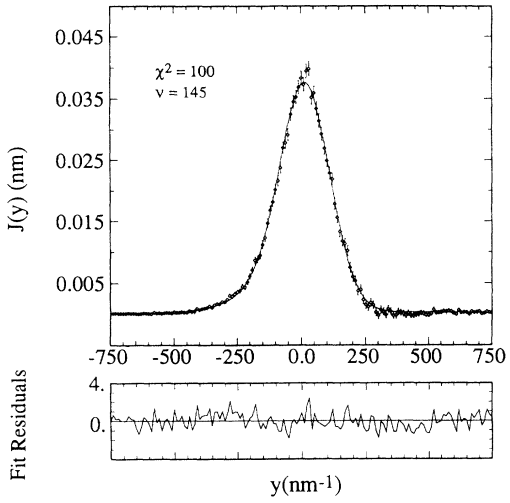

FIG. 7. 101.2° data and fit for solid Ar at 42.3 K.

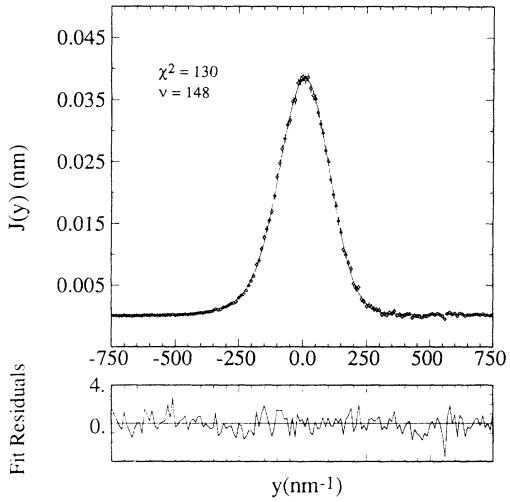

FIG. 8. 101.2° data and fit for solid Ar at 46.6 K.

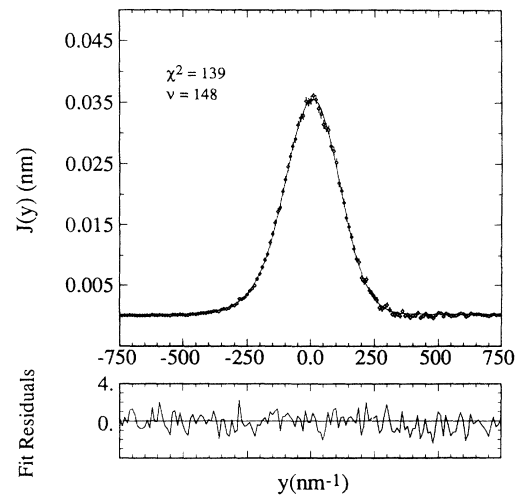

FIG. 9. 101.2° data and fit for solid Ar at 73.0 K. Compare the overall broadening due to temperature with the data shown in Fig. 5.

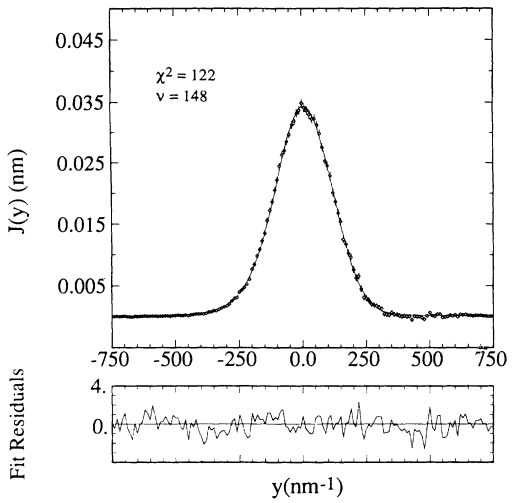

FIG. 10. 101.2° data and fit for liquid Ar at 84.9 K.

solid Ar at all temperatures. The mean-squared displacements determined from the classical Monte Carlo and molecular-dynamics calculations do not take into account quantum zero-point motion so they do have not have the correct low-temperature behavior. The quasiharmonic calculations of $\langle u^2 \rangle$ are limited by the fact that the perturbation theory used breaks down at temperatures greater than one-half the melting temperature. The SCP mean-squared displacements are listed in Table II. Also listed in Table II are the Debye-Waller factors calculated, using Eq. (21), for $Q=192$ nm^{-1}, the smallest wave-vector transfer data analyzed.

In the fitting process the scattering intensity of the function representing the ^{36}Ar response was constrained to be 62.5% of the intensity of the function representing the ^{40}Ar response (Table I). Several other constraints were employed during the fitting process: (i) For the 84.9-K liquid sample the single-particle kinetic energies of the Ar isotopes were constrained to be the same; (ii) For the solid-Ar samples a self-consistent-average-phonon[23] model, discussed in the Appendix, was used to relate the kinetic energies of ^{36}Ar and ^{40}Ar; and (iii) the separation of the peak centers was fixed at a value determined from the scattering kinematics.

A low-order background polynomial was also used in the fits to the data of the three lower-temperature solid samples. Its inclusion was found to significantly improve the quality of the fits as measured by the reduced χ squared. A possible interpretation of this small background is that it accounts for sample-dependent scattering not described by the fitting function. Additional multiple scattering is expected as the temperature of the sample is decreased due to an increase in the sample density. The density of the lower-temperature samples is approximately 30% greater than that of the 110.6-K liquid which was used to generate the fitting functions for the lower-temperature samples. Therefore, one expects the fitting functions not to account for all the sample-dependent multiple scattering for the lower-temperature samples.

TABLE II. Mean-squared displacements and Debye-Waller factors as a function of temperature for solid Ar at $Q=192$ nm^{-1}. The values of $\langle u^2 \rangle$ are from Ref. 21.

Temperature (K)	$\langle u^2 \rangle$ (nm^{-2})	Debye-Waller factor
0	3.6×10^{-4}	1.20×10^{-2}
15	4.2×10^{-4}	5.74×10^{-3}
30	6.0×10^{-4}	6.28×10^{-4}
45	8.5×10^{-4}	2.91×10^{-5}
60	1.20×10^{-3}	3.95×10^{-7}
75	1.63×10^{-3}	2.00×10^{-9}

IV. RESULTS AND DISCUSSION

For a given temperature, $\langle E_k \rangle$ was determined for each detector bank; the average over all detector banks is listed in Table III. The uncertainty in $\langle E_k \rangle$ is estimated by combining the uncertainty in the fitted width for each detector bank with the standard deviation of $\langle E_k \rangle$ determined from the fitted widths. We now compare our results with the predictions of several models and $\langle E_k \rangle$ values inferred from data obtained with other experimental techniques (Fig. 11, Tables IV and V).

A. Inelastic (low-Q) data

Using a triple-axis spectrometer for coherent inelastic neutron scattering two groups have measured phonon frequencies and line shapes in solid ^{36}Ar. Eckert and Youngblood performed such measurements at 81 K, close to melting ($T_m=83.7$ K) along the [100] and [110] directions.[7] Fujii *et al.* did so at 10 K along the [100], [110], and [111] directions.[6] Both groups determined force constants for the solid from the observed phonon energies with Born–von Kármán models. Eckert and Youngblood fitted their data with a third-neighbor axially symmetric force model, while Fujii *et al.* used a third-neighbor general force model. With the force constants determined the phonon density of states $g(\omega)$ can be calculated by means of the Gilat and Raubenheimer method.[24] Knowledge of the phonon density of states allows $\langle E_k \rangle$ to be determined in the harmonic approximation, in which $\langle E_k \rangle$ is half the total vibrational energy,

$$\langle E_k \rangle = \tfrac{1}{2} \int_0^\infty g(\omega)[n(\omega,T)+\tfrac{1}{2}]\hbar\omega \, d\omega \, , \tag{22}$$

where

$$n(\omega,T)=\frac{1}{\exp(\hbar\omega/k_B T)-1} \, . \tag{23}$$

TABLE III. Experimental values of $\langle E_k(T) \rangle$ for condensed ^{40}Ar.

Reference	Temperature (K)	$\langle E_k \rangle$ (K)	Uncertainty (%)
Present work	18.3	54.3	4
Present work	28.2	62	7
Present work	42.3	78	6
Present work	46.6	81	5
Present work	73.0	113	4
Ref. 1	82.0	121	7
Present work	84.9	129	2

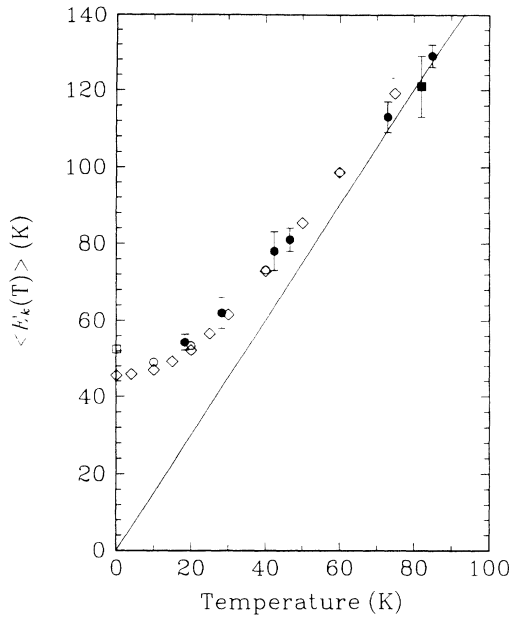

FIG. 11. Single-particle kinetic energy in condensed Ar. The solid circles are our measured values. The solid square is the experimental value from Ref. 1. Various theoretical results are open circles (PIMC, Ref. 27), open diamonds (EPMC, Ref. 28), and open square (variation, Ref. 31). The solid line is the equipartition prediction $(3/2)k_B T$.

With the $g(\omega)$ from Refs. 6 and 7, $\langle E_k \rangle$ values at 10 and at 81 K, respectively, were computed for ^{36}Ar (see Table IV). Comparison of these $\langle E_k \rangle$ with our measured ^{40}Ar $\langle E_k \rangle$ values shows at 81 K (if one interpolates between our data points) the agreement is good. At low temperature the agreement is not as good. In addition, as shown in Table V, the $\langle E_k \rangle$ of ^{40}Ar is approximately 5% less than the $\langle E_k \rangle$ of ^{36}Ar at 10 K. One therefore finds the value of $\langle E_k \rangle$ at 10 K determined from Eq. (22) is somewhat lower than an extrapolation of our data would yield.

B. Calorimetric data estimate

In solid Ne deep-inelastic-neutron-scattering measurements have shown the single-particle ground-state kinetic energy $\langle E_k(0) \rangle$ constitutes 60% of the total ground-state vibrational energy predicted from the Debye model,[25]

$$\langle E_{\text{vib}}(0) \rangle = (\tfrac{9}{8})\theta_D^0 , \quad [\theta_D^0(\text{Ne}) = 74.6 \text{ K}] . \tag{24}$$

This result is interpreted as indicating anharmonic contributions to $\langle E_k(0) \rangle$ are appreciable in solid Ne, because the measured calorimetric value of θ_D^0 already contains the anharmonic frequency shifts of the long-wavelength phonons.

From a precise published value of θ_D^0 for Ar,[26] one obtains the value for $\langle E_k(0) \rangle$ given in Table IV.

One may estimate $\langle E_k(0) \rangle$ in Ar from our data by an extrapolation using either the values given by effective potential Monte Carlo (EPMC) calculation (Sec. IV C) or by the SCAP model (Appendix). For example, subtracting the SCAP *difference* between $\langle E_k \rangle$ at 0 and 18.3 K from our measured $\langle E_k(18.3) \rangle$ value yields $\langle E_k(0) \rangle = 51.9 \pm 2.1$ K. This $\langle E_k(0) \rangle$ is 50±2% of the total ground-state vibrational energy predicted from the Debye model $[\theta_D^0(\text{Ar}) = 92.0 \text{ K}]$.[26] The difference in the relative amounts of ground-state kinetic energies between solid Ar and Ne can be ascribed to the difference in the dynamics of the atoms. For example, in the SCAP model, zero-point excursions from the equilibrium positions in a Ne lattice at zero temperature are 6% of the nearest-neighbor distance, while in Ar such excursions are approximately 3%. From our results it appears the effect of anharmonicity on $\langle E_k(0) \rangle$ in solid Ar is smaller than in solid Ne.

TABLE IV. Calculated values of $\langle E_k \rangle$. See text Sec. IV.

Reference	Temperature (K)	$\langle E_k \rangle$ (K)
Debye Model[a]	0	51.8
Bernardes[b]	0	54.1
Silvi *et al.*[c]	0	52.5
Eckert and Youngblood[d]	10.0	49.6
Fujii *et al.*[e]	81.0	126.7

[a]For ^{40}Ar. From Eq. (24), with Debye temperature from Ref. 26.
[b]Reference 29. Uses Lennard-Jones parameters from Ref. 16.
[c]Reference 31.
[d]For ^{36}Ar. Computed using the density of states from Ref. 7.
[e]For ^{36}Ar. Computed using the density of states from Ref. 6.

TABLE V. Ratio of $\langle E_k(^{36}\text{Ar}) \rangle$ to $\langle E_k(^{40}\text{Ar}) \rangle$ from the SCAP model.

Temperature (K)	$\langle E_k(^{36}\text{Ar}) \rangle / \langle E_k(^{40}\text{Ar}) \rangle$
18.3	1.047
28.2	1.031
42.3	1.018
46.6	1.016
73.0	1.007

C. Path integral and effective potential Monte Carlo results

Path-integral Monte Carlo (PIMC) calculations of $\langle E_k \rangle$ in solid Ar have been computed at four temperatures under the assumption that the Lennard-Jones potential[16] adequately represents the effective pair potential of solid Ar.[27] The results are shown in Fig. 11. At all but the lowest temperature the PIMC values agree rather well with our measured $\langle E_k \rangle$ results. At low temperatures the PIMC results for $\langle E_k \rangle$ are smaller than the zero-temperature Debye Model results [Eq. (24)] and the SCAP model using the same potential (Table VI).

Effective potential Monte Carlo (EPMC) calculations of $\langle E_k \rangle$ in solid Ar have also been published.[28] These are also shown in Fig. 11. These lie even lower than the PIMC values using the same Lennard-Jones potential.[16] The difference is greater at lower temperatures.

TABLE VI. Values of $\langle E_k \rangle$ for ^{40}Ar from the SCAP model, using the same Lennard-Jones parameters as in Refs. 27, 28, and 29.

Temperature (K)	$\langle E_k \rangle$ (K)
0	51.1
18.3	53.4
28.2	60.8
42.3	76.1
46.6	81.3
73.0	116.3

D. Variational calculations

An early calculation of $\langle E_k \rangle$ in solid Ar at zero temperature is that of Bernardes.[29] In this work the Einstein model is applied to the noble-gas solids Ne, Ar, Kr, and Xe by assuming uncorrelated single-particle trial variational wave functions. The Lennard-Jones potential is used to represent the interatomic potential and the results are presented in terms of the parameters σ and ε. A value $\langle E_k(0) \rangle$ of 54.1 K is obtained using values for the potential parameters from Ref. 16 (Table IV).

A Hartree calculation employing the more realistic two-body potential of LeSar[30] has been performed by Silvi *et al.*[31] Assuming the single-particle Ar wave function is Gaussian and evaluating lattice sums out to fifth-nearest neighbors, Silvi *et al.* determined the center-of-mass oscillation frequency of the Ar atoms. The zero-point $\langle E_k \rangle$ corresponding to this frequency is 52.5 K (Table IV). This is in good agreement with the extrapolation of our experimental results to zero temperature.

E. A note on potentials

A Lennard-Jones potential is not the correct pair potential for Ar. Regardless, it is often argued that such a simple form is possibly an approximate suitable representation of the total potential in condensed Ar.[27,28,32] Alternatively, in some theory papers, the form is admitted to be unrepresentative of Ar, but nevertheless is used so that the results can be directly compared to previously published model calculations.

In order to achieve very close agreement with the measured phonon frequencies and equation-of-state of solid Ar, theorists have turned to more sophisticated pair potentials,[33] for example, the Aziz-Chen potential,[34] plus the inclusion of multibody forces. These multibody forces may be taken to have the form of the Axilrod-Teller-Muto (ATM) triple-dipole interaction. It is known that inclusion of the ATM interaction in quasiharmonic theory leads to an increase of 0.7% in the calculated zero-point energy.[35] At higher temperatures one expects the effects of multibody forces to diminish due to decreasing sample density. The precision of the present measurements does not permit effects of this magnitude to be observed, but we note that the difference between our measured values of $\langle E_k \rangle$ and those of PIMC and EPMC calculations using a Lennard-Jones potential has this qualitative behavior.

V. CONCLUSION

The atomic kinetic energy of condensed Ar has been determined over a wide range of temperature via deep-inelastic-neutron scattering. For the first time, it has been demonstrated that accurate $\langle E_k(T) \rangle$ values can be obtained for a heavy-mass system whose scattering significantly overlaps that of the sample container. There is qualitative agreement with some published theoretical calculations, but there are differences in detail. Increased precision in similar inelastic measurements should be obtainable with instruments with better resolution.

Ar is a popular host matrix for studies of guest molecules and free radicals.[36] Directly measured temperature dependence for the kinetic energy of Ar provides evidence for the use in the interpretation of such experiments, for example, studies of guest H_2 molecules.[37]

ACKNOWLEDGMENTS

This research was supported by the U.S. Department of Energy, BES-Materials Sciences under Contract No. DE-FG02-91ER45439. It has benefited from the use of the Intense Pulsed Neutron Source (IPNS) at Argonne National Laboratory. This facility is funded by the U.S. Department of Energy, BES-Materials Sciences, under Contract No. W-31-109-ENG-38. We are pleased to acknowledge the able assistance of the staff of IPNS. We thank R. C. Blasdell for use of data reduction software and M. E. Mostoller for use of The Oak Ridge National Laboratory phonon density-of-states code. One of us (R.O.S.) thanks Professor J. Peisl for his hospitality in Munich and the Alexander von Humboldt Foundation for support in Germany.

APPENDIX: SELF-CONSISTENT-AVERAGE-PHONON (SCAP) MODEL

One model which predicts $\langle E_k \rangle$ over a broad range of temperatures is the self-consistent-average-phonon model (SCAP).[23] The SCP approach[21] is followed to determine temperature-dependent phonon frequencies, but in the SCAP model, averages over functions of the phonon frequencies are replaced by functions of a temperature-dependent *average phonon* frequency. This greatly reduces the numerical complexity of the SCP formalism, while still producing a renormalization of phonon frequencies due to lattice anharmonicity. The self-consistent equations of SCAP are

$$\langle u^2 \rangle = \frac{3\hbar}{2M\langle \omega^2 \rangle^{1/2}} \coth\left[\frac{\hbar\langle \omega^2 \rangle^{1/2}}{2k_B T}\right], \tag{A1}$$

and

$$\langle \omega^2 \rangle = \frac{1}{3M}\left[S_2 + \frac{S_4}{3}\langle u^2 \rangle + \frac{4S_6}{(3)4!}\langle u^2 \rangle^2\right], \tag{A2}$$

with

$$S_n = \sum_i \left[\frac{d^n V}{dR_{0i}^n} + \frac{n}{R_{0i}}\frac{d^{(n-1)}V}{dR_{0i}^{(n-1)}}\right], \tag{A3}$$

where R_{0i} is the mean position of the ith atom relative to a given origin atom, $\langle u^2 \rangle$ is the mean-squared atomic displacement, ω is the phonon frequency, and $\langle \cdots \rangle$ denotes a thermal average. The temperature-dependent single-particle kinetic energy is

$$\langle E_k \rangle_{\mathrm{SCAP}} = \tfrac{1}{2} M \langle u^2 \rangle \langle \omega^2 \rangle \ . \tag{A4}$$

The SCAP model illustrates why $\langle u^2 \rangle$ is not directly proportional to $\langle E_k \rangle$. As can be seen in Eqs. (A1)–(A4) higher powers of $\langle u^2 \rangle$ contribute to $\langle E_k \rangle$. In a harmonic system $\langle E_k \rangle$ would be proportional to $\langle u^2 \rangle$ and would be one-half the total vibrational energy of the atom.

In our SCAP calculation, for computational simplicity we used the Lennard-Jones parameters of Ref. 16 (*not* those of Ref. 23) and precise lattice parameter results.[38] The ratio of $\langle E_k(^{36}\mathrm{Ar}) \rangle$ to $\langle E_k(^{40}\mathrm{Ar}) \rangle$ for this model is shown in Table V. From Tables III and VI, agreement between $\langle E_k \rangle_{\mathrm{SCAP}}$ and our measured values of $\langle E_k \rangle$ is good at all temperatures, which provides a self-consistent check on this correction.

We also calculated the SCAP S_2 term [see Eqs. (A2) and (A3)] using the Aziz-Chen HFD-C2 potential.[34] The resulting zero-point $\langle E_k(0) \rangle$ is 0.9 K less than that obtained when the Lennard-Jones potential[16] was used to calculate all terms. At 83 K the difference in $\langle E_k \rangle$ is 0.2 K. At a minimum, this illustrates that possible systematic uncertainty, beyond any statistical uncertainties given, is present in published values of $\langle E_k \rangle$, which use a Lennard-Jones form.

*Present address: Department of Physics and Astronomy, Colgate University, 13 Oak Drive, Hamilton, NY 13346-1398.

†Permanent address: Department of Physics, University of Illinois at Urbana-Champaign, 1110 West Green Street, Urbana, IL 61801-3080.

[1]D. A. Peek and R. O. Simmons, J. Chem. Phys. **94**, 3169 (1991).

[2]R. O. Simmons, Z. Naturforsch. **48a**, 415 (1993).

[3]See, for example, D. C. Wallace, *Thermodynamics of Crystals* (Wiley, New York, 1972) and *Rare Gas Solids,* edited by M. L. Klein and J. A. Venables (Academic, New York, 1976 and 1977), Vols. 1 and 2.

[4]A very brief preliminary account appeared in M. A. Fradkin, S.-X. Zeng, and R. O. Simmons, Z. Naturforsch. **48a**, 438 (1993).

[5]H. A. Egger, M. Gsanger, E. Lüscher, and B. Dorner, Phys. Lett. **28A**, 433 (1968); D. N. Batchelder, M. F. Collins, B. C. G. Haywood, and G. R. Sidey, J. Phys. C **3**, 249 (1970); D. N. Batchelder, B. C. G. Haywood, and D. H. Saunderson, *ibid.* **4**, 910 (1971).

[6]Y. Fujii, N. A. Lurie, R. Pynn, and G. Shirane, Phys. Rev. B **10**, 3647 (1974).

[7]J. Eckert and R. W. Youngblood, Phys. Rev. B **34**, 2770 (1986).

[8]V. F. Sears, Phys. Rev. **30**, 44 (1984).

[9]See, for example, A. S. Rinat and M. V. Butler, Phys. Rev. B **41**, 11 149 (1990), which contains other relevant references ranging back to H. A. Gersch and L. J. Rodriguez, Phys. Rev. A **8**, 905 (1973).

[10]V. F. Sears, Can. J. Phys. **63**, 68 (1985).

[11]L. H. Nosanow and G. L. Shaw, Phys. Rev. **128**, 546 (1962). This calculation is restricted to quadratic terms in the atomic displacements.

[12]R. C. Blasdell, Ph.D. thesis, University of Illinois at Urbana-Champaign, 1992 (unpublished).

[13]D. N. Batchelder, D. L. Losee, and R. O. Simmons, in *Crystal Growth* (Pergamon, New York, 1967), p. 843; B. A. Fraass, S. M. Heald, and R. O. Simmons, J. Cryst. Growth **42**, 370 (1977).

[14]V. F. Sears, Phys. Rev. A **7**, 340 (1973).

[15]L. Verlet, Phys. Rev. **159**, 98 (1967).

[16]A. Michels, Hub. Wijker, and Hk. Wijker, Physica **15**, 627 (1949).

[17]C.-K. Loong, S. Ikeda, and J. M. Carpenter, Nucl. Instrum. Methods Phys. Res. A **260**, 381 (1987).

[18]A. Sjölander, Ark. Fys. **14**, 315 (1958).

[19]The determination of mean-squared displacements is an active area of research. See, for example, H. R. Schober, Philos. Mag. Lett. **66**, 159 (1992).

[20]V. V. Goldman, Phys. Rev. **174**, 1041 (1968).

[21]L. B. Kanney, J. Low Temp. Phys. **12**, 239 (1973).

[22]G. A. Heiser, R. C. Shukla, and E. R. Cowley, Phys. Rev. B **33**, 2158 (1986).

[23]K. Shukla, A. Paskin, D. O. Welch, and G. J. Dienes, Phys. Rev. B **24**, 724 (1981); A. Paskin, A.-M. Llois de Kreiner, K. Shukla, D. O. Welch, and G. J. Dienes, Phys. Rev. B **25**, 1297 (1982).

[24]G. Gilat and L. J. Raubenheimer, Phys. Rev. **144**, 390 (1966).

[25]D. A. Peek, I. Fujita, M. C. Schmidt, and R. O. Simmons, Phys. Rev. B **45**, 9680 (1992).

[26]L. Finegold and N. E. Phillips, Phys. Rev. **177**, 1383 (1969).

[27]A. Cuccoli, A. Macchi, M. Neuman, V. Tognetti, and R. Vaia, Phys. Rev. B **45**, 2088 (1992).

[28]A. Cuccoli, A. Macchi, V. Tognetti, and R. Vaia, Phys. Rev. B **47**, 14 923 (1993).

[29]N. Bernardes, Phys. Rev. **112**, 1534 (1958).

[30]R. LeSar, J. Phys. Chem. **88**, 4272 (1984).

[31]B. Silvi, V. Chandrasekharan, M. Chergui, and R. D. Etters, Phys. Rev. B **33**, 2749 (1986).

[32]G. C. Maitland, M. Rigby, E. B. Smith, and W. A. Wakeham, *Intermolecular Forces, Their Origin and Determination* (Clarendon, Oxford, 1987).

[33]J. A. Barker, in *Simple Molecular Systems at Very High Density,* edited by A. Polian, P. Loubeyre, and N. Boccara (Plenum, New York, 1989), p. 341.

[34]R. A. Aziz and H. H. Chen, J. Chem. Phys. **67**, 5719 (1977). See also, R. A. Aziz, in *Inert Gases: Potentials, Dynamics and Energy Transfer in Doped Crystals,* edited by M. L. Klein (Springer-Verlag, Berlin, 1984).

[35]M. V. Bobetic and J. A. Barker, Phys. Rev. B **2**, 4169 (1970).

[36]*Inert Gases: Potentials, Dynamics, and Energy Transfer in Doped Crystals,* edited by M. L. Klein (Springer-Verlag, Berlin, 1984).

[37]K. W. Herwig and R. O. Simmons, in *Momentum Distributions,* edited by R. N. Silver and P. E. Sokol (Plenum, New York, 1989), p. 203.

[38]O. G. Petersen, D. N. Batchelder, and R. O. Simmons, Phys. Rev. **150**, 703 (1966).